chapter seven

MAGNETIC INTERACTIONS

in copper proteins and copper complexes

CONTENTS

7.1	*Theory and practice*	*143-145*
7.2	*G-tensors of copper complexes*	*146-152*
7.3	*Hyperfine splittings*	*153-156*
7.4	*Copper proteins*	*157-161*

SUMMARY

The calculation of g-tensors and hyperfine coupling tensors of copper complexes and copper proteins by DFT studies is presented in Chapter 7. It is shown that a procedure is needed in order to get reasonable agreement between computed and experimental g-tensor values. The computed copper hyperfine coupling constants are sometimes in disagreement with the experimental values, but in many cases a good agreement is observed. For the other atoms, especially in wildtype azurin, a good agreement is found between the computed and experimental hyperfine couplings.

7.1 Theory and practice

Magnetic interactions of electrons and molecular systems, in particular copper containing systems

If a free atom carries a magnetic dipole moment μ, it will interact with a magnetic field B, which is described by the Hamiltonian $\mathcal{H}$:[16,282,283]

$$\mathcal{H} = \mu \cdot B \tag{1}$$

One source of a magnetic moment in an atom is orbital electronic motion that results directly from the angular momentum l of the charge. For an electron moving in an orbit, μ_L is found to have the classical value:

$$\mu_L = (-e/2mc)l \tag{2}$$

where l is its orbital angular momentum, e the charge and m the mass of the electron, and c the velocity of light. This illustrates the generality that μ is proportional to angular momentum, but oppositely directed, for a negatively charged electron. This proportionality is often expressed by the definition of the magnetogyric ratio γ:

$$\mu = \gamma l \tag{3}$$

The electron also spins about its own axis, i.e. it has an intrinsic magnetic moment, but here μ_e is anomalously larger due to spin orbit coupling, by a factor of 2, than for μ_L:

$$\mu_s = 2(-e/2mc)s \tag{4}$$

These orbital and spin contributions are then added to give the total magnetic moment of the atom.

The solution of eq. (1) yields the energy U of the magnetic particle in the field as:

$$U = -\mu B \cos\theta \tag{5}$$

where θ is the angle between the dipole moment μ and the static magnetic field B. Classically, the energy can vary continuously with the orientation of the magnetic moment; quantum mechanically, this is quantized and the angle can take only $2J+1$ orientations, where J is the quantum number for total angular momentum. The allowed projections of J (or μ) along the magnetic field direction are given by m_J, where m_J is the magnetic quantum number with the values:

$$m_J = J, J-1, \ldots, -J \tag{6}$$

If only spin angular momentum arises (as in an atom in a $^2S_{1/2}$ state), m_J becomes:

$$m_s = S, S-1, \ldots, -S \tag{7}$$

with the total electron spin quantum number S. The moment μ_z along the field direction is then (as $l_S = m_S\hbar$):

$$\mu_z = -2(e\hbar/2mc)m_s \tag{8}$$

With the definition of the Bohr magneton μ_B as $e\hbar/2mc$, the (Zeeman) allowed energies for an atom in a magnetic field are found:

$$U_{m_s} = -\mu_z B = 2\mu_B m_s B \tag{9}$$

Thus, in this pure spin case, the familiar equal spacing of 2S+1 energy levels occurs with a separation of $2\mu_B B$.

For a free electron, a small quantum electrodynamics correction requires that this equation be written as:

$$U_{m_s} = g_e \mu_B m_s B \tag{10}$$

where g_e is 2.0023. In this case, $m_J = m_S = \pm 1/2$ and only two Zeeman levels are possible. By applying an oscillating magnetic field of frequency ν_0 perpendicular to B, a transition can be induced from one level to the other, at a particular resonance B_0 (see Figure 7.1.1):

$$h\nu_0 = g_e \mu_B B_0 \tag{11}$$

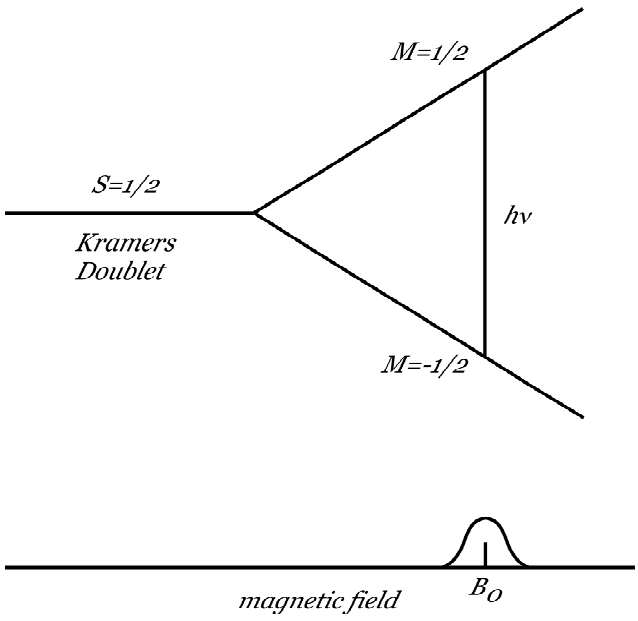

FIGURE 7.1.1. ZEEMAN SPLITTING AND RESONANCE

This is applied in the field of Electron Spin or Paramagnetic Resonance (ESR/EPR), where the strength of the static magnetic field is varied to find the position of the resonance, which results in an EPR spectrum.

Effective spin Hamiltonian

For an electron bound to a copper complex, it is possible to set up an effective spin Hamiltonian in a quantum mechanical formulation as:

$$\hat{\mathcal{H}} = \square_B \left(\mathbf{B} \cdot \mathbf{g} \cdot \hat{\mathbf{S}} \right) \tag{12}$$

where $\mathcal{H}$ is the operator that, when applied to the wavefunctions of the system, gives the energy eigenvalues. The spin operator vector **S** refers to the effective spin of magnitude 1/2 for the copper complex, and **g** is the g-matrix that describes the interaction of the orbital and spin angular momenta via the spin-orbit coupling. It is symmetric, e.g. $g_{x\,y}=g_{y\,x}$, and the **g**-tensor may be diagonalized by an appropriate choice of the x, y and z directions.

Another important interaction in the spin Hamiltonian is the nuclear hyperfine interaction, which arises from the interaction of the nuclear magnetic moments and the magnetic field at the nuclei generated by the magnetic electrons. As the copper nucleus has a nuclear spin I of 3/2, each electron spin level is split into four components with values of the z component of the nuclear spin quantum number m of −3/2, −1/2, +1/2, +3/2. Thus, the electron resonance line is split into four approximately equally spaced components with a splitting of approximately A, which is the magnitude of the nuclear hyperfine interaction. It has a directional dependence and is therefore more generally written as:

$$\mathcal{H}_{hf} = \mathbf{S} \cdot \mathbf{A} \cdot \mathbf{I} \tag{13}$$

where **I** is the nuclear spin operator vector and **A** the hyperfine interaction matrix, which can be diagonalized by an appropriate choice of axes. In general, these axes are not the same as found for the **g**-tensor, but sometimes they are.

Some more sophisticated additions can be made for the spin Hamiltonian, like the interaction of the nuclear quadrupole moment, but these effects are usually smaller, and may be ignored as a first approximation.

Typical g_z values for copper complexes are of the order of 2.1-2.6, with a hyperfine splitting of ~0.02 cm^{-1}. As already mentioned in Section 1.2, copper proteins are classified according to three types:

- type 1 copper proteins contain one copper ion, exhibit an unusual EPR spectrum with a hyperfine splitting appreciably smaller than that found for simple copper complexes. They exhibit an intense blue color, g_z values of 2.2-2.3 and hyperfine splittings around ~0.003-0.008 cm^{-1}.
- type 2 copper proteins exhibit EPR spectra similar to those of simple copper complexes.
- type 3 copper proteins contain a dinuclear copper site and usually, as isolated, are EPR silent, which means that the copper atoms are either in the reduced form, or antiferromagnetically coupled. There are no pronounced features in the optical spectrum visible.

7.2 G-tensors of copper complexes

Prediction of g-tensors of copper molecules by Density Functional Theory calculations

In this section g-tensors are predicted using Density Functional Theory[1] calculations. In the recent literature, it has been reported that it may be difficult to obtain reliable g-tensor values with DFT for complexes containing metal atoms[284-287], although in certain instances a good agreement between calculated and experimental values is observed[288-291]. In this section, a number of copper complexes is used to check the influence on the accuracy of the predicted g-tensors of several issues related to the DFT calculations, like the size of the basis set, (non-) relativistic Hamiltonian, exchange-correlation potential, and the method by which the g-tensor is calculated. Furthermore, the influence of the copper nuclear charge on the results is investigated, as it has been suggested as a possible way to improve the results. The prediction of hyperfine splitting tensors of these molecules is presented in Section 7.3, while the g- and A-tensors for the active sites of copper proteins are described in Section 7.4.

Computational details

Implementations in the ADF code

There are two implementations available in the ADF code[117] for obtaining the g-tensor of a system (with a total spin of 1/2). The first one (ESR), developed by van Lenthe et al.[284,292], uses Gauge Including Atomic Orbitals (GIAO), where the g- and A-tensors are calculated in a Spin-Orbit relativistic calculation using either the Pauli or the more preferred ZORA Hamiltonian[117]. Although the g-tensor can only be calculated in a Spin-Orbit relativistic calculation, the g-tensor of a non-relativistic or scalar relavistic run can still be obtained by using the density from the latter in a Spin-Orbit calculation. The other implementation[291,293] (EPR) is available as an analysis tool, which should be run in a separate program after performing a normal ADF job, which should be either relativistic with the Pauli Hamiltonian or non-relativistic. This implementation does not provide the hyperfine splitting tensor.

Molecule set

A total of eight molecules has been studied[a], for which a comparison of the calculated g- and A-tensors can be made to either experimental data[282,294-296] or other calculated tensors. The geometries of the molecules were taken at their experimental values where available[190,282,297,298], while the remaining unknown coordinates were optimized with the Becke[120]-Perdew[121] potential using a triple zeta valence plus polarization basis in a non-relativistic run of the ADF program.

---

[a] The molecules are: $CuCl_4^{2-}$ (square planar D_{4h} geometry), $Cu(CO)_3$ (trigonal D_{3h} geometry), CuF_2 (linear), $Cu(H_2O)_6^{2+}$ (D_{2h} symmetry), CuH^+ (linear), $Cu(NO_3)_2$ (D_{2h} symmetry), $CuNO^+$ and CuO (linear)

Results

The principal g-tensor values of a number of copper complexes are given in Table 7.2.1. These values were calculated with Density Functional Theory using the Becke[120]-Perdew[121] exchange-correlation potential in a triple zeta valence plus polarization basis set. The values from both the ESR- and EPR implementations are given where available; for CuO and CuF2 the ESR method was unable to provide the values, as a set of degenerate orbitals was found. This inability has also been found for the EPR implementation, when using the same orbitals from a restricted run. In a subsequent unrestricted run, where the alpha- and beta-orbitals are no longer constrained to be the same, the EPR implementation did provide the g-tensor.

Given in Table 7.2.1 are the ESR values from either a non-relativistic calculation where the ZORA Hamiltonian has been used in the Spin-Orbit calculation for obtaining the g-tensor (nr-zora), a scalar relativistic run using ZORA (sr-zora), a non-relativistic run where the Pauli Hamiltonian was used in the Spin-Orbit run (nr-pauli), a scalar relativistic run using the Pauli Hamiltonian (sr-pauli), and the EPR values from either a non-relativistic run (nr-epr) or a scalar relativistic run using the Pauli Hamiltonian (sr-epr). For the ESR calculations, also the g-tensor from a full Spin-Orbit calculation was obtained, but the difference from the one obtained from the scalar relativistic run is small; the principal values were constantly smaller in the full Spin-Orbit run, but by an amount of less than 0.1.

The deviations from the free electron value (2.0023) of the calculated principal values of the g-tensors are in nearly all cases smaller than observed in experiments. For copperchlorate ($CuCl_4^{2-}$), the deviation from the free electron value is experimentally found to be ~0.22, while the DFT calculations predict a deviation of only ~0.09 (40 %). The same underestimation of the deviation is observed for other molecules like $Cu(NO_3)_2$ (0.12 calculated vs. 0.25 experimental) or $CuNO^+$ (–0.06 calculated vs. –0.11 experimental). The deviations from the free electron value of the principal value from the EPR implementation are similar or smaller than the ones from the ESR implementation. This is only in part due to the different Hamiltonians used (Pauli or ZORA). For comparison, the g-tensors of the Pauli Hamiltonian in the ESR implementation are also given in Table 7.2.1. The Pauli principal values from the ESR implementation differ more from those obtained in the EPR implementation than the values from ZORA/ESR.

In a recent investigation[71] to study the g-tensor of *wildtype* azurin, it was shown that an effective core potential (ECP) description was needed for copper, which included implicitly relativistic corrections. As the inclusion of the ECP on copper improved the calculated g-tensors considerably (from ~2.10 to ~2.23), it was suggested that relativistic corrections may be needed for copper. However, for the copper complexes studied here a rather small difference is observed between the values from a non-relativistic and a (scalar/Spin-Orbit) relativistic calculation, where the principal values of the g-tensor differ by approximately 0.01-0.02 or less. This small influence of relativistic corrections could have been anticipated for a first row transition metal like copper. Although the molecules in this section are smaller than the active site model of *wildtype* azurin, the rather small difference between non-relativistic and relativistic calculations on the copper complexes seems to suggest that relativistic corrections may improve the g-tensors slightly, but might be not the major factor for the underestimation of the g-tensor principal values.

The dependence of the g-tensor on the basis set size can not be ignored completely. In Table 7.2.2, the principal values of the g-tensor from the ESR implementation are given in three basis sets; a small double zeta valence basis (DZV), a medium triple zeta valence plus

polarization basis (TZP) and a large quadruple zeta basis set (QZ). Upon increasing the basis set size from DZV to TZP, the deviation of g-tensor principal values from the free electron value decreases by a small amount in most cases.

TABLE 7.2.1. G-TENSORS FOR BECKE-PERDEW POTENTIAL IN TZP BASIS

	exp.	*nr-zora*[a]	*sr-zora*[b]	*nr-epr*[c]	*sr-epr*[d]	*nr-pauli*[e]	*sr-pauli*[f]
$CuCl_4^{2-}$							
g_x	*2.040*	2.029	2.030	2.032	2.033	2.035	2.036
g_y	*2.040*	2.029	2.030	2.032	2.033	2.035	2.036
g_z	*2.221*	2.087	2.096	2.092	2.096	2.125	2.138
$Cu(CO)_3$							
g_x	*2.0002*	2.0004	2.0011	2.0002	2.0006	1.9990	1.9999
g_y	*2.0002*	2.0004	2.0011	2.0002	2.0006	1.9990	1.9999
g_z	*2.0008*	2.0018	2.0019	2.0009	2.0008	2.0009	2.0009
CuF2							
g_x	*2.601*	-[g]	-[g]	2.244	2.231	-[g]	-[g]
g_y	*2.601*	-[g]	-[g]	2.244	2.231	-[g]	-[g]
g_z	*1.913*	-[g]	-[g]	2.003	2.003	-[g]	-[g]
$Cu(H_2O)_6^{2+}$							
g_x	*2.095*	2.054	2.060	2.059	2.059	2.064	2.074
g_y	*2.095*	2.075	2.077	2.066	2.066	2.095	2.098
g_z	*2.40*	2.287	2.300	2.214	2.216	2.406	2.426
CuH^+							
g_x	-	2.122	2.147	2.094	2.116	2.179	2.213
g_y	-	2.122	2.147	2.094	2.116	2.179	2.213
g_z	-	1.997	1.995	2.002	2.002	1.990	1.987
$Cu(NO_3)_2$							
g_x	*2.052*	2.025	2.028	2.030	2.031	2.033	2.038
g_y	*2.052*	2.027	2.031	2.032	2.033	2.035	2.041
g_z	*2.249*	2.113	2.126	2.117	2.119	2.162	2.180
$CuNO^+$							
g_x	*2.009*	2.010	2.014	2.006	2.005	2.013	2.018
g_y	*2.009*	2.013	2.017	2.009	2.009	2.017	2.023
g_z	*1.89*	1.939	1.938	1.961	1.965	1.924	1.921
CuO							
g_x	-	-[g]	-[g]	2.049	2.046	-[g]	-[g]
g_y	-	-[g]	-[g]	2.049	2.046	-[g]	-[g]
g_z	-	-[g]	-[g]	2.002	2.002	-[g]	-[g]

a) Non-relativistic density, g-tensor calculated with ZORA Spin-Orbit Hamiltonian
b) Scalar relativistic density, g-tensor calculated with ZORA Spin-Orbit Hamiltonian
c) Non-relativistic unrestricted density, g-tensor calculated with EPR program
d) Pauli Scalar relativistic unrestricted density, g-tensor calculated with EPR program
e) Non-relativistic density, g-tensor calculated with Pauli Spin-Orbit Hamiltonian
f) Scalar relativistic density, g-tensor calculated with Pauli Spin-Orbit Hamiltonian
g) No results available; breakdown due to degenerate orbitals

Increasing the basis set size even more to QZ leads to an increase again, giving in many cases larger deviations from the free electron value than the small DZV basis. For instance for hydrated copper, the scalar relativistic g-tensor z-value goes from 2.32 (DZV) to 2.30 (TZP) to 2.35 (QZ) upon increasing the basis set. For CuH^+ on the other hand, a very small dependence of the g-tensor on the basis is observed. Generally speaking, the best results are

obtained in the large QZ basis, but a rather similar result can be obtained in the DZV or TZP basis.

TABLE 7.2.2. G-TENSORS FOR BECKE-PERDEW POTENTIAL IN THREE BASIS SETS

	exp.	*nr-dzv*	*nr-tzp*	*nr-qz*	*sr-dzv*	*sr-tzp*	*sr-qz*
$CuCl_4^{2-}$							
g_x	*2.040*	2.030	2.029	2.031	2.031	2.030	2.032
g_y	*2.040*	2.030	2.029	2.031	2.031	2.030	2.032
g_z	*2.221*	2.091	2.087	2.098	2.100	2.096	2.110
$Cu(CO)_3$							
g_x	*2.0002*	1.9993	2.0004	2.0016	2.0000	2.0011	2.0025
g_y	*2.0002*	1.9993	2.0004	2.0016	2.0000	2.0011	2.0025
g_z	*2.0008*	2.0019	2.0018	2.0018	2.0019	2.0019	2.0018
$Cu(H2O)6^{2+}$							
7 g_x	*2.095*	2.061	2.054	2.064	2.066	2.060	2.070
g_y	*2.095*	2.076	2.075	2.082	2.079	2.077	2.086
g_z	*2.40*	2.305	2.287	2.334	2.317	2.300	2.349
CuH^+							
g_x	-	2.120	2.122	2.130	2.145	2.147	2.160
g_y	-	2.120	2.122	2.130	2.145	2.147	2.160
g_z	-	1.997	1.997	1.996	1.996	1.995	1.994
$Cu(NO3)2$							
g_x	*2.052*	2.024	2.025	2.028	2.027	2.028	2.032
g_y	*2.052*	2.027	2.027	2.030	2.031	2.031	2.034
g_z	*2.249*	2.113	2.113	2.129	2.127	2.126	2.145
$CuNO^+$							
g_x	*2.009*	2.013	2.010	2.014	2.017	2.014	2.019
g_y	*2.009*	2.013	2.013	2.012	2.017	2.017	2.016
g_z	*1.89*	1.910	1.939	1.932	1.909	1.938	1.931

nr) non-relativistic
sr) scalar relativistic (ZORA)
dzv) double zeta valence basis set
tzp) triple zeta valence plus polarization basis set
qz) quadruple zeta valence basis set

The choice of using the Becke-Perdew (BP) exchange-correlation potential could also have an influence on the calculated g-tensor values. Therefore the g-tensors for the molecules were also calculated for four other potentials; the standard local density approximation (LDA), Perdew-Burke-Ernzerhof[228] (PBE) potentials, as well as two potentials that have been specially constructed for an accurate description of excitation energies and (hyper)polarizabilities: statistical averaging of orbital potentials[299] (SAOP) and the gradient regulated asymptotically corrected[300] (GRAC) potential. As these last two potentials seem to give a better description of the (HOMO-LUMO) orbital energies, they might have a marked effect on the g-tensor values also. The computed g-tensor principal values for these five exchange-correlation potentials in the DZV basis set are given in Table 7.2.3. The difference between the principal g-tensor values from the five potentials is of the same order of magnitude as the difference between the different basis sets. For instance for copperchlorate, the computed principal z-value of the g-tensor with either one of the five potentials ranges from 2.096 to 2.111, which is almost exactly the range observed for the

three different basis sets. For hydrated copper, the principal z-value of the g-tensor is computed in the range from 2.317 to 2.344 for the same potentials. This again is almost exactly the range that is observed for the three different basis sets. Therefore, just like the size of the basis set, also the choice of the exchange-correlation is shown to have only a small effect on the computed g-tensors.

Only a small difference is observed between the BP and GRAC results. As the latter is a gradient regulated combination of the BP potential for the inner region and the asymptotically correct LB94 potential for the outer region, this indicates that the outer region is not really that important for a description of the g-tensor. This behavior is observed for all three basis sets used (DZV, TZP and QZ).

TABLE 7.2.3. G-TENSOR PRINCIPAL VALUES FOR XC-POTENTIALS IN DZV BASIS

	exp.	*lda*	*bp*	*pbe*	*saop*	*grac*
$CuCl_4^{2-}$						
g_x	*2.040*	2.030	2.031	2.031	2.032	2.031
g_y	*2.040*	2.030	2.031	2.031	2.032	2.031
g_z	*2.221*	2.096	2.100	2.103	2.107	2.100
$Cu(CO)_3$						
g_x	*2.0002*	2.0004	2.0000	1.9999	1.9991	2.0002
g_y	*2.0002*	2.0004	2.0000	1.9999	1.9991	2.0002
g_z	*2.0008*	2.0019	2.0019	2.0019	2.0019	2.0019
$Cu(H_2O)_6^{2+}$						
g_x	*2.095*	2.062	2.066	2.066	2.071	2.066
g_y	*2.095*	2.076	2.079	2.080	2.086	2.076
g_z	*2.40*	2.335	2.317	2.325	2.338	2.317
CuH^+						
g_x	-	2.143	2.145	2.144	2.157	2.144
g_y	-	2.143	2.145	2.144	2.157	2.144
g_z	-	1.995	1.996	1.996	1.995	1.995
$Cu(NO_3)_2$						
g_x	*2.052*	2.026	2.027	2.027	2.030	2.027
g_y	*2.052*	2.030	2.031	2.031	2.035	2.031
g_z	*2.249*	2.122	2.127	2.128	2.139	2.127
$CuNO^+$						
g_x	*2.009*	2.010	2.017	2.017	2.017	2.017
g_y	*2.009*	2.012	2.017	2.018	2.024	2.017
g_z	*1.89*	1.884	1.909	1.902	1.882	1.910

Adjustment of the nuclear charge on copper

It has been suggested by Groenen and Solomon[a] that a possible way of improving the computed g-tensor values is by changing the nuclear charge of copper. The assumption is that the copper 3d orbitals are too low in energy to mix properly with the ligand orbitals, thereby producing a too low contribution of copper orbitals in the singly occupied molecular orbital (SOMO). The adjustment of the copper nuclear charge would effectively push the 3d-orbitals on copper upwards, leading to larger contributions of copper orbitals in the highest occupied molecular orbitals (including the SOMO), which would lead to increased z-values of

[a] E.J.J. Groenen, E.I. Solomon, personal communication

the g-tensor. Alternatively, this procedure would also lead to improved excitation energies (see Chapter 8).

For the same set of molecules, the nuclear charge on copper has been adjusted in steps of 0.2 electron, shifting it downwards from 29.0 to 28.2. The computed principal g-tensor values in the DZV basis set using the Becke-Perdew xc-potential are given in Table 7.2.4. As expected, the principal values of the g-tensor increase with decreasing copper nuclear charge. This pattern is not only observed for the z-values of the g-tensor, but also for the x- and y-values.

For CuH^+, some difficulties arise when adjusting the copper nuclear charge. Just like found for CuF_2 and CuO, some molecular orbitals become degenerate with certain copper nuclear charges, leading to erroneous g-tensors.

TABLE 7.2.4. G-TENSOR VALUES AS FUNCTION OF COPPER NUCLEAR CHARGE (Z)

	exp.	*Z=29.0*	*Z=28.8*	*Z=28.6*	*Z=28.4*	*Z=28.2*
$CuCl_4^{2-}$						
g_x	*2.040*	2.031	2.039	2.053	2.070	2.084
g_y	*2.040*	2.031	2.039	2.053	2.070	2.084
g_z	*2.221*	2.100	2.141	2.187	2.232	2.271
$Cu(CO)_3$						
g_x	*2.0002*	2.0000	2.0015	2.0030	2.0044	2.0058
g_y	*2.0002*	2.0000	2.0015	2.0030	2.0044	2.0058
g_z	*2.0008*	2.0019	2.0019	2.0019	2.0019	2.0019
$Cu(H_2O)_6^{2-}$						
g_x	*2.095*	2.066	2.078	2.096	2.104	2.098
g_y	*2.095*	2.079	2.091	2.108	2.110	2.110
g_z	*2.40*	2.317	2.347	2.396	2.417	2.426
CuH^+						
g_x	-	2.145	2.218	2.283[a]	2.195	2.316[b]
g_y	-	2.145	2.218	2.283[a]	2.195	2.316[b]
g_z	-	1.996	1.990	1.983[a]	1.993	1.983[b]
$Cu(NO_3)_2$						
g_x	*2.052*	2.027	2.037	2.047	2.051	2.045
g_y	*2.052*	2.031	2.044	2.059	2.073	2.083
g_z	*2.249*	2.127	2.161	2.191	2.215	2.231
$CuNO^+$						
g_x	*2.009*	2.017	2.023	2.026	2.028	2.029
g_y	*2.009*	2.017	2.026	2.039	2.056	2.078
g_z	*1.89*	1.909	1.912	1.918	1.925	1.935

a) g-tensor from non-relativistic density

b) value obtained in TZP basis

Based on the g_z-values with the largest deviation from the free electron value (copper chlorate, hydrated copper and copper dinitrate), the "optimal" value of the copper nuclear charge for the prediction of good g-tensors would then be around 28.4-28.6, depending on which basis set one uses. For TZP a value of 28.4 seems more appropriate, for QZ a value of 28.6 while it is somewhere inbetween for the DZV basis. These "optimal" values seem to be rather insensitive to the xc-potential used. In the following section, the prediction of

hyperfine splitting A-tensors is discussed for the same molecules, while the application to the active sites of copper proteins is presented in Section 7.4.

Conclusions

The computed g-tensors of copper complexes using Density Functional Theory are, without using special procedures to improve the results, rather disappointing. Generally speaking, only half of the experimental deviation from the free electron value is recovered by the calculations. Including scalar or spin-orbit relativistic effects or increasing the basis set size have only a marginal, yet improving, effect.

The computed values can be improved by artificially lowering the copper nuclear charge, which has the effect that effectively the copper d-orbitals are shifted upwards and the contributions of these in the singly occupied highest occupied molecular orbital are increased. This effectively leads to larger g-tensor values and therefore to a better agreement with experimental data.

7.3 *Hyperfine splittings*

Prediction of the A-tensor of copper complexes

In Section 7.2, the prediction of the g-tensor of copper complexes has been discussed, while in this section the calculation of hyperfine splitting (A-) tensors is presented. Unlike the g-tensors for which one value is obtained for the whole quantum system, the A-tensors are obtained per atom. The tensors are best obtained in an unrestricted calculation, e.g. a calculation where the Kohn-Sham orbitals for the alpha- and beta-electrons, and therefore the alpha- and beta-spin density, are not constrained to be the same.

TABLE 7.3.1. XC-POTENTIAL DEPENDENCE OF HYPERFINE SPLITTINGS[a] (MHZ)

	exp.[282,301]	*LDA*	*BP*	*PBE*	*SAOP*	*GRAC*
$CuCl_4^{2-}$						
Cu	-234	-152	-183	-179	-316	-188
Cl	-	24	24	24	9	24
$Cu(CO)_3$						
Cu	71	-11.3	-0.8	-0.5	345	20.4
C	-18.7	-19.4	-20.9	-17.3	6	-14.0
O	-11.2	4.6	0.7	-1.0	-70	-6.2
CuF_2						
Cu	2038[b]	-273	-229	-	-	-227
F	240[b]	-123	-77	-	-	-82
$Cu(H_2O)_6^{2+}$						
Cu	-	-175	-190	-189	-531	-195
O_{ax}	-	3	4	4	3	2
O_{eq}	-	-101	-97	-97	-80	-98
CuH^+						
Cu	-	3223	2972	-	3519	2964
H	-	517	532	-	860	532
$CU(NO_3)_2$						
Cu	-223	-209	-239	-233	-335	-245
O	-	-2	-6	-8	26	-7
N	-	-4	-3	-3	7	-3
$CuNO^+$						
Cu	570	2548	2470	2412	2366	2448
N	-	42	42	45	-17	43
O	-	18	5	-1	72	2
CuO						
Cu	-484	-807	-718	-663	-1138	-645
O	-	52	37	24	307	37

a) isotropic value of hyperfine splitting tensor in DZV basis set
b) absolute value

In Section 7.2, it was shown that the choice of the exchange-correlation potential had little effect on the calculated g-tensor values. Whether this is true also for the hyperfine

splitting tensor, is examined first. The computed isotropic values of the A-tensor for the same five xc-potentials (LDA[119], BP[120,121], PBE[228], SAOP[299] and GRAC[300]) as used in Section 7.2 are given in Table 7.3.1.

Apart from the SAOP potential, only relatively small differences are observed between the five xc-potentials. For instance for copper chlorate, the isotropic hyperfine splitting value of ranges from –152 to –188 MHz copper and is 24 MHz on chloride for all potentials; for hydrated copper the isotropic hyperfine splitting ranges from –175 to –195 MHz on copper and from –97 to –101 MHz on the equatorial oxygen. For CuH^+ some larger differences are observed on copper (2964 to 3223 MHz), but for hydrogen the value remains rather constant at 517-532 MHz. Still, these larger differences are still small compared to the difference between the molecules, and may therefore not be significant.

In most cases, the order of magnitude of the isotropic hyperfine splittings is correct in comparison with the experimental value, apart from the copper hyperfine splitting in CuF_2 and $CuNO^+$. In the former, the computed values are too small by a factor of 7-8, while in the latter, the computed values are too large by factor of 4-5.

TABLE 7.3.2. BASIS SET DEPENDENCE OF HYPERFINE SPLITTINGS[a] (MHZ)

	exp. [282,301]	*DZV*	*TZP*	*QZ*
$CuCl_4^{2-}$				
Cu	-234	-183	-183	-248
Cl	-	24	27	29
$Cu(CO)_3$				
Cu	71	-0.8	-17.8	-8.0
C	-18.7	-20.9	-14.7	-16.4
O	-11.2	0.7	-5.4	-3.0
CuF_2				
Cu	2038	-229	-213	-282
F	240	-77	-81	49
$Cu(H_2O)_6^{2+}$				
Cu	-	-190	-182	-
O_{ax}	-	4	3	-
O_{eq}	-	-97	-96	-
CuH^+				
Cu	-	2972	3016	3237
H	-	532	469	477
$CU(NO_3)_2$				
Cu	223	-239	-238	-316
O	-	-6	-21	-17
N	-	-3	-4	-3
$CuNO^+$				
Cu	570	2470	2940	3170
N	-	42	48	44
O	-	5	-21	-11
CuO				
Cu	-484	-718	-661	-677
O	-	37	-25	-6

a) isotropic value of hyperfine splitting tensor using Becke-Perdew potential

The influence of the choice of basis set on the computed values is checked using the Becke-Perdew potential in the same three basis sets that have been used in Section 7.2 (small DZV, medium TZP and large QZ basis sets). The computed isotropic hyperfine splitting values are given in Table 7.3.2. It is observed that the basis set size has some effect on the computed isotropic hyperfine splitting values, but not the dramatic changes needed to get good values compared to the experimental results. This could have been anticipated, as the influence of the basis set on the computed g-tensor values was shown to be small. For $CuNO^+$, the copper hyperfine splitting increases from 2470 MHz in the DZV basis to 3170 MHz in the QZ basis set, and thereby reduces the agreement with the experimental value even more. On the other hand for copper chlorate, the difference between the computed and experimental value decreases to only 10 MHz.

TABLE 7.3.3. HYPERFINE SPLITTINGS[a] (MHZ) AS FUNCTION OF NUCLEAR CHARGE Z

atom	*exp.*	*Z=29.0*	*Z=28.8*	*Z=28.6*	*Z=28.4*	*Z=28.2*
$CuCl_4^{2-}$						
Cu	-234	-183	-186	-196	-217	-247
Cl	-	24	29	33	35	36
$Cu(CO)_3$						
Cu	71	-0.8	-2.1	-2.8	-3.1	-3.3
C	-18.7	-20.9	-20.5	-20.1	-19.6	-19.1
O	-11.2	0.7	0.7	0.6	0.6	0.6
CuF_2						
Cu	2038	-229	-237	-249	-263	-273
F	240	-77	-55	-38	-28	-26
$Cu(H_2O)_6^{2+}$						
Cu	-	-190	-191	-	-	-326
O_{ax}	-	4	4	-	-	43
O_{eq}	-	-97	-89	-	-	-94
CuH^+						
Cu	-	2972	334	138	25	-18
H	-	532	205	149	88	31
$CU(NO_3)_2$						
Cu	-223	-239	-241	-250	-267	-290
O	-	-6	-13	-19	-24	-28
N	-	-3	-3	-2	-2	-3
$CuNO^+$						
Cu	570	2470	2557	2696	2846	2961
N	-	42	38	37	36	37
O	-	5	5	4	3	2
CuO						
Cu	-484	-718	-656	-616	-567	-534
O	-	37	32	27	22	19

a) isotropic hyperfine splitting tensor value in DZV basis with Becke-Perdew potential

In Section 7.2, it was observed that a special procedure was needed to get reasonable agreement between computed and experimental g-tensor values. This procedure consisted of lowering the nuclear charge on copper, which would effectively shift the d-orbitals of copper upwards. This leads to larger contributions of these orbitals in the singly occupied

molecular orbital of the unpaired electron, and therefore to increased g-tensor values. The influence of this procedure on the computed isotropic hyperfine splitting values is reported in Table 7.3.3. The computed isotropic hyperfine splitting values show different trends for different molecules; for some, the values get more negative, for others they get more positive. The most striking example in this case is CuH^+, in which the copper hyperfine splitting changes from 2972 MHz to –18 MHz, while for hydrogen it changes from 532 MHz to 31 MHz.

The drastic improvement of the computed g-tensor values is however not accompanied by an evenly drastic improvement of the hyperfine splittings. The molecules for which the hyperfine splitting values were already properly described, remain to be so when using this procedure, while for the molecules for which a discrepancy exists between the experimental and computed values, also remain being so. Just like was observed for using the larger QZ basis set, using the special procedure, that helped to improve the computed g-tensor, reduces the agreement between the computed and experimental value of for instance $CuNO^+$.

Conclusions

The hyperfine splitting (A-) tensor of the atoms in copper complexes is computed using Density Functional Theory calculations. The computed values are in most cases of the right order of magnitude in comparison with the experimental values, but in some cases a large discrepancy exists between the two. Although the computed values may vary to some extent by using different basis sets and/or exchange-correlation potentials, the changes in computed values are relatively small. The molecules for which a reasonable agreement between computed and experimental values was observed, remain being properly described, while the molecules that showed a large discrepancy between experimental and computed values, remain to do so.

The special procedure used in Section 7.2 to give a drastic improvement of the computed g-tensor values, has a small effect on the computed hyperfine splitting values, about the same order of magnitude observed when using a different basis set and/or exchange-correlation potential. Therefore, although it has a major impact on the g-tensor values, the influence on the hyperfine splitting values is relatively small, apart from the CuH^+ molecule, in which the copper hyperfine splitting value changes from 2972 MHz to –18 MHz, and the hydrogen value from 532 MHz to 31 MHz.

7.4 Copper proteins

Prediction of g-tensors and hyperfine splittings of (models of) the active sites of copper proteins

Until now in this chapter the computation of g-tensors and hyperfine splitting values has been limited to copper complexes, to check whether the computed values are in general agreement with the experimental ones, and to see how they can be improved. In this section, the computation of g-tensors and hyperfine splittings of (active sites of) copper proteins will be presented and discussed. Based on the experience in the previous sections with the choice of the basis set and/or exchange-correlation potential, which was shown to have a small effect, the Becke[120]-Perdew[121] potential is used in a DZV basis set. The potential has been used throughout the rest of the thesis as well, while the calculations will be finished faster when using this smaller basis set.

Several models for the active sites of copper proteins can be thought of, the simplest being simply a copper and a cysteinate (*model 1*). As this ligand is present in all type 1 copper proteins, and its presence is thought to be responsible to a great extent for the strong blue color and the characteristic EPR-features, it might be interesting to see how the computed EPR-parameters compare with larger active site models and experiments. The second model consists apart from the cysteinate also of the other two strong histidine ligands (*model 2*). This model has also been used in an investigation by van Gastel et al.[71] to study the EPR-parameters for wildtype azurin. They observed that it was necessary to use an effective core potential (ECP) on copper that includes relativistic corrections. As the use of the ECP improved the computed g-tensors considerably, it was concluded that relativistic effects should be included to get a good description of the g-tensor. However, as was shown in Section 7.2, the inclusion of (scalar or spin-orbit) relativistic effects in DFT calculations has only a limited effect on the computed g-tensor. The values do shift upwards, but only by 0.01 or 0.02. The major impact of using the ECP is to shift the copper d-orbitals upwards, just like observed for the lowering of the copper nuclear charge.

The first two models can more or less be used as typical models for type 1 copper proteins. More realistic active site models are obtained if also the axial ligands are included in the calculations (*model 3*). In that case, one should be able to distinguish different proteins like *wildtype* azurin, M121Q or M121H azurin. In all these models the amino acid residues are cut off at the carbon-alpha position with the backbone connections replaced by hydrogens.

G-tensors

The computed principal g-tensor values for the models are listed in Table 7.4.1, again also using the suggested procedure (involving a lowering of the copper nuclear charge) to improve the computed values. In Section 7.2, it was shown that a value around 28.4-28.6 for the copper nuclear charge seemed appropriate to calculate reasonably accurate g-tensors for copper complexes. Assuming that the same trend is observed in copper proteins, the g-tensors were calculated using the normal charge (29.0) as well as the ones that performed best for the copper complexes (28.4 and 28.6).

Just like was found for the copper complexes, using a lower copper nuclear charge shifts the computed g-tensor values upwards, to values that compare well with experimental values. This pattern is observed for all models, except the most simple one (*model 1*). In that case, the lowering of the copper nuclear charge has a negligible effect, and seems to even lower the computed g-tensor values. Apparently, the interaction with the histidines is necessary to get a more balanced distribution of the unpaired electron.

TABLE 7.4.1. G-TENSORS OF ACTIVE SITE MODELS (WITH CU NUCLEAR CHARGE Z)

	exp.	*Z=29.0*	*Z=28.6*	*Z=28.4*
model 1:				
g_x	-	2.031	2.021	2.002
g_y	-	2.095	2.046	2.019
g_z	-	2.119	2.093	2.042
model 2:				
g_x	-	2.028	2.059	2.081
g_y	-	2.077	2.092	2.109
g_z	-	2.111	2.244	2.310
model 3:				
g_x *wt*	$2.039^{74,302\text{-}304}$	2.029	2.088	2.124
g_y *wt*	$2.057^{74,302\text{-}304}$	2.072	2.111	2.143
g_z *wt*	$2.273^{74,302\text{-}304}$	2.126	2.278	2.338
g_x *m121q*	2.028^{38}	2.033	2.063	2.085
g_y *m121q*	2.083^{38}	2.072	2.102	2.121
g_z *m121q*	2.288^{38}	2.108	2.199	2.238
g_x *m121h*	2.051^{23}	1.976	1.881	1.806
g_y *m121h*	2.056^{23}	1.999	1.938	1.865
g_z *m121h*	2.265^{23}	2.081	2.172	2.296
g_x *m121e_p*[a]	2.03^{77}	2.027	1.920	2.002
g_y *m121e_p*[a]	2.085^{77}	2.063	2.028	2.016
g_z *m121e_p*[a]	2.30^{77}	2.120	2.219	2.070
g_x *m121e_dp*[b]	2.06^{77}	-	-	2.017
g_y *m121e_dp*[b]	2.06^{77}	-	-	2.137
g_z *m121e_dp*[b]	2.30^{77}	-	-	2.200

a) m121e_p: Glu121 protonated
b) m121e_dp: Glu121 deprotonated

A different behavior is observed for wildtype azurin and M121Q azurin regarding the g_z value; the values are found to be higher for the former than for the latter. For wildtype azurin, a good agreement between the computed g_z value (using a copper nuclear charge of 28.6) and the experimental value is found. Although the g_x and g_y values are somewhat larger than found experimentally, the computed difference between the two (0.023) is again in good agreement with the experimental value of 0.018. The M121Q mutant shows much more rhombic values, with a computed difference between the g_x and g_y values (0.039) that is almost twice as large as for wildtype azurin. This is again in good agreement with the

experimental data (0.055) that indicate a rhombic EPR spectrum, although the g_z value is too small compared to the experimental value.

For the M121H mutant, unexpected results are obtained; the g_x and g_y values are in all cases even below the free electron value of 2.0023. The same is observed for the M121E mutant, for which g-tensor values are obtained at two different pH values (at pH=4 and pH=8); at low pH, the Glu121 residue is protonated at the $O_{\varepsilon 2}$ position, while it is deprotonated at high pH. Preliminary calculations using the TZP basis set, with the same result, seem to indicate that this unexpected behavior is not due to the relatively small basis set used.

Hyperfine splitting tensors

The hyperfine splitting tensors have been computed, just like in the previous section, in a spin-unrestricted run. The computed isotropic hyperfine splittings are given in Table 7.4.2 for copper and some other atoms.

TABLE 7.4.2. ISOTROPIC HYPERFINE SPLITTING[a] (MHZ) OF ACTIVE SITE MODELS

	Cu	O_{45}	$N_{46,\delta}$	$N_{46,\varepsilon}$	S_{112}	$N_{117,\delta}$	$N_{117,\varepsilon}$	X_{121}[b]
model 1	-276.7	-	-	-	-5.9	-	-	-
model 2	-167.8	-	14.4	0.8	-1.3	20.3	1.4	-
model 3:								
wt	-157.5	0.1	16.1	0.9	-0.3	22.4	1.5	-2.1
m121q	-89.7	0.3	17.6	1.3	-1.3	28.7	1.7	0.7
m121h	-59.9	0.0	13.2	0.3	-1.4	30.4	1.9	10.2
m121e_p[c]	-119.8	1.0	19.4	1.1	-0.4	26.1	1.8	-2.9
m121e_dp[d]	-88.8	0.7	22.6	1.5	-0.4	26.5	2.1	-11.1

a) computed values in DZV basis with copper nuclear charge of 28.6;
b) X=S, O, N
c) m121e_p: Glu121 protonated
d) m121e_dp: Glu121 deprotonated

Compared to model 1, the copper hyperfine splitting decreases upon inclusion of the histidine residues in model 2, as well as the hyperfine splitting on sulphur. Including also the axial ligands in model 3 (*wt*) even decreases the values even some more. Still, the values for copper is too large by a factor of three compared to experimental data. However, the principal values of the A-tensor are, relatively speaking, in good agreement with experimental data, which show in both cases a large value in the z-direction and almost negligible values in the x- and y-direction.

The computed hyperfine splittings of the nitrogens in the histidine residues in the *wt* structure agree very well with the experimental values of 18.1 (N_δ-His46), 0.9 (N_ε-His46), 25.1 (N_δ-His117) and 1.3 MHz (N_ε-His117). Also the hydrogen hyperfine couplings are in good agreement (see Table 7.4.3). The largest values are found for the H_β protons of Cys112, with computed values of 31.5 and 28.2 MHz that agree very well with the experimental values of 27 and 28 MHz. Also the hyperfine coupling of the H_α of Cys112 is well described (−0.4 MHz

for both the experimental and computed value). The hyperfine couplings of the protons in the histidines are reasonably well described; there is either a good agreement (for instance for $H_{\varepsilon 1/\varepsilon 2}$-His46, $H_{\delta 2}$-His46) or agreement within the limit of the accuracy of both methods.

The isotropic hyperfine couplings of copper in the M121Q, M121H and M121E mutants is considerably lower than in *wildtype* azurin. The hyperfine coupling of the other atoms doesn't change significantly apart from the atom in residue 121 in the M121H and *deprotonated* M121E mutants, where the absolute value increases to roughly 10 MHz.

TABLE 7.4.3. COMPARISON OF PROTON HYPERFINE COUPLINGS (MHZ) OF PROTONS IN ACTIVE SITE OF *WILDTYPE* AZURIN

proton	*experimental*	*computed*
H δ2 His46	1.49	0.79
H ε1 His46	1.06/1.48	1.32
H ε2 His46	0.56	0.60
H β1 Cys112	28/27	31.5
H β2 Cys112	27/28	28.2
H α Cys112	-0.38	-0.44
H δ2 His117	1.61	2.00
H ε1 His117	1.45/1.02	0.79
H ε2 His117	-	1.06

For the Met121Glu mutant, two different sets of hyperfine tensors are observed on copper, one at low pH where Glu121 is protonated and one at high pH where Glu121 is deprotonated. Even though the principal values of the g-tensor change by only a relatively small amount, the principal values of the hyperfine coupling tensor change dramatically. In the protonated form the A_x value (182 MHz) is larger than the A_z value (70 MHz), while in the deprotonated form the A_x value (28 MHz) is smaller than the A_z value (232 MHz). Even though the computed values are too large in the absolute sense, the same pattern is observed with values of 453/109 MHz (A_x/A_z) in the protonated form and 214/427 MHz (A_x/A_z) in the deprotonated form.

Conclusions

The g-tensor and atomic hyperfine couplings were computed for several active site models of copper proteins and the results compared with experimental data. For the g-tensor a reasonable agreement is observed for *wildtype* azurin and the M121Q mutant, especially when looking which type of spectra (rhombic/axial) is observed, but peculiar results are obtained for the M121H and M121E mutants. Further investigation is needed for these mutants, which is currently being done.

The hyperfine coupling of copper is too large by a factor of three, but the relative principal values of the A-tensor are well described, with a large value in the z-direction and almost negligible values in the x- and y-direction. The hyperfine couplings of the nitrogen

atoms in the histidine residues show a good agreement between the experimental and computed values, with larger values observed in the His117 residue. Also the relative values of the N_δ vs. the N_ε atoms is well described. Also for the protons in the histidine and cysteine residues is a good agreement between experimental and computed values observed for *wildtype* azurin.

In the Met121Glu mutant of azurin two sets of experimental data are available, corresponding to Glu121 being either protonated or deprotonated; the principal values of the copper hyperfine tensor change dramatically in relative values. In the protonated form, the hyperfine coupling in the x-direction is largest, while in the deprotonated form the hyperfine coupling in the z-direction is largest. Apart from the fact that the computed values are too large by a factor of roughly three, the same change in relative values is observed.